https://ntrs.nasa.gov/search.jsp?R=19890006582 2020-03-20T03:34:41+00:00Z

N89-15953

EVALUATION OF ERBE SCANNER POINTING ACCURACY BASED UPON A COASTLINE DETECTION ALGORITHM

William L. Weaver, Lawrence H. Hoffman, and James F. Kibler
Atmospheric Sciences Division
NASA Langley Research Center
Hampton, Virginia 23665-5225

ABSTRACT

Measurements from the Earth Radiation Budget Experiment (ERBE) scanning radiometers must be accurately located at the top of the Earth's atmosphere for proper interpretation of derived longwave and shortwave components of the Earth radiation field. The accuracy of the location calculations is affected by the orbit characteristics and attitude control systems of the three spacecraft, ERBS, NOAA-9, and NOAA-10. A technique was developed which makes use of the longwave scanner measurements to detect the thermal gradients at the boundaries of ocean and land masses. By analyzing many such coastline boundaries, estimates of the overall accuracy of the scanner measurement location calculations have been derived for the three satellites. The resulting measurement location errors are found to be smaller than the resolution of the radiometers, and this accuracy is well within the required location knowledge for useful science analysis of the ERBE scanner data.

EVALUATION OF ERBE SCANNER POINTING ACCURACY BASED UPON A COASTLINE DETECTION ALGORITHM

William L. Weaver, Lawrence H. Hoffman, and James F. Kibler
Atmospheric Sciences Division
NASA Langley Research Center
Hampton, Virginia 23665-5225

INTRODUCTION

The Earth Radiation Budget Experiment (ERBE) instruments are operating on three Earth-orbiting spacecraft. The Earth Radiation Budget Satellite (ERBS) operated by the National Aeronautics and Space Administration (NASA) at the Goddard Space Flight Center (GSFC), is in a 600-km, 57° inclination orbit with a precessional period of about 2 months. The National Oceanic and Atmospheric Administration (NOAA) satellites NOAA-9 and NOAA-10, launched in December 1984 and September 1986, respectively, are in about 860- and 825-km Sun-synchronous orbits, each with a different local time for its nodal crossing. Each ERBE instrument set consists of fixed field-of-view (non scanning) and cross-track scanning radiometers. The overall ERBE mission concept and design is described in reference 1, and the ERBE scanner and non scanner instruments are described in references 2 and 3, respectively.

In deriving Earth radiation fields from the ERBE radiation measurements, both the surface characteristics at the measurement location on the Earth and the satellite-Earth-Sun geometry play important roles. The task of accurately calculating the Earth locations for the ERBE measurements is complicated by the fact that there is no imaging system associated with the ERBE measurements, and thus, landmark identification is difficult. Therefore, a concerted effort was made to understand the process by which the Earth locations of measurements are calculated, and a technique was developed for verifying the accuracy of the calculations. Because of the more rigorous accuracy requirements of the scanner instruments, this paper is concerned only with the measurements from the scanners. The scanner instruments make instantaneous radiance measurements in three broad spectral bands: shortwave, longwave, and total as the scan head traverses a path normal to the orbit ground track every 4 seconds.

The Earth-location verification technique developed makes use of the scanner radiometric measurements to detect sharply contrasting thermal regions on the Earth which occur at the boundaries of water and land masses. This paper describes the steps in computing the measurement locations and the development of the verification technique and its application to assessing the accuracy of the ERBE measurement locations.

CALCULATION OF EARTH LOCATIONS OF ERBE SCANNER INSTRUMENT MEASUREMENTS

The primary objective of the ERBE experiment is to determine the monthly average radiant exitances at the top of the atmosphere (TOA) over the Earth with a resolution of 250 km. Figure 1, which is an example of a typical monthly product, is the map of the average longwave exitance for April 1985 derived from ERBE scanner measurements made from the ERBS spacecraft. The production of this end product, starting with computing the radiances from the individual scanner measurements at the spacecraft, inverting the radiances to flux densities at the TOA, and then averaging over time and space, is discussed in reference 4.

The accuracy of these derived exitances depends on correctly calculating the locations on the Earth of the source of each of the individual scanner radiometric measurements. This calculation is done in two major steps. The first major step is to transform a pointing vector in the detector coordinate system to one in a local geodetic system. Figure 2 is a schematic of the scanner instrument which illustrates its coordinate systems, and figure 3 illustrates the instantaneous local geodetic (or horizon) system at the spacecraft. The X-axis of the local geodetic system is along the component of the velocity vector in the geodetic plane (V_x) , the Y-axis is normal to the orbit plane, and the Z-axis is along the local geodetic nadir. The pointing vector for the scanner measurement is derived as follows: The unit vector along the optical axis of the detector is transformed from detector coordinates into pedestal coordinates by rotating through the instrument elevation and azimuth angles; the resulting vector is transformed into the coordinates of the specific spacecraft; and finally, this vector is transformed into the local geodetic system by rotating through the spacecraft orientation or attitude angles. Some salient points in this process are given here, and the details are described in reference 5.

Special attention was given at each stage of instrument manufacturing and buildup and in the process of mating the instruments with their respective spacecraft to ensure proper alignment of components which affect the calculation of detector pointing vectors. The decision was made to use the actual values of the instrument elevation and azimuth beam angles for calculating the location of each measurement instead of deriving these angles by modeling the motion of the instrument elevation angles. This, we believe, significantly increased the accuracy of the measurement locations. The instrument azimuth and elevation beam angles are edited during processing to ensure correct values before calculating the pointing vector. The frequency of occurrence of the instrument azimuth beam angles in the telemetry data stream is much lower than that of the radiometric measurements, and pointing vectors are not computed if the azimuth beam is in motion.

Both the ERBS and NOAA spacecraft use a combination of horizon sensors, inertial gyros, and Sun sensors to keep the spacecraft aligned with the local geodetic system

of figure 3. The three spacecraft attitude angles are provided in the telemetry data as deviations from these instantaneous coordinate axes, and the attitude angles are used in the final transformation of the pointing vector into the local geodetic coordinates. The quantities required to define the local geodetic system of figure 3 and to transform the scanner pointing vector from that system into an Earth-fixed system are derived from orbit ephemeris data. The ephemeris data for both the ERBS and the NOAA spacecraft are calculated by GSFC, and these ephemeris data have been found to be very accurate.

The second major step in calculating the Earth location of a scanner measurement starts by transforming the pointing vector from the local geodetic system to Earth-fixed coordinates using the spacecraft heading angle. The associated spacecraft ephemeris data are transformed from the inertial frame to the same Earth- fixed coordinate system and are interpolated to the time of the scanner measurement. The details of these transformations are described in reference 5.

The final task is to determine the intersection of the pointing vector with the Earth's surface. The Earth's surface is modeled by an ellipsoid, and the geometry of the pointing vector intersection with the ellipsoid is illustrated in figure 4. In this figure, R_e and R_p are the equatorial and polar radii of the Earth and h is the altitude of the TOA above the Earth's surface. Given a vector from the center of the Earth to the spacecraft ($\mathbf{P}$) and a detector unit pointing vector ($\hat{\mathbf{V}}$) the magnitude of the vector from the spacecraft to the intersection with the ellipsoid ($\mathbf{V}$), is determined using relationships described in reference 5. The final result is the estimated latitude and longitude of the center of the measurement point on the surface of the Earth.

METHOD OF ASSESSING MEASUREMENT LOCATION ACCURACY

The method described above is used in the ERBE processing system to calculate the Earth location of every scanner radiometric measurement. Now, a technique is needed to evaluate how successfully the method locates the scanner measurements. One way to assess the accuracy is to identify Earth features using the scanner radiometric measurements. The shortwave radiometric measurements are not used because they have large variations due to clouds and are not useful at night. When there are large thermal contrasts, the longwave measurements show thermally interesting features such as desert adjacent to an ocean. Points on this thermal boundary between the desert and ocean can be identified making use of multiple scan cycles of scanner radiometric data. The points on the coastline determined by this method can then be compared to an actual map, and errors in the latitude and longitude of the estimated location point can be estimated. Coastline identification results for many days and several sites are then accumulated in scatter plots which illustrate both the random errors and biases in the locations of the detected coastlines.

In selecting suitable coastlines for use in applying the coastline detection algorithm, the following characteristics were considered important to its successful application:

(a) Probable high thermal contrast between land and water.
(b) Infrequent cloud cover.
(c) No unusual terrain features, such as lakes and mountains, next to the coastline.
(d) Interesting coastline. An absolutely straight coastline is not adequate for detecting errors along the coastline. A coastline with regular curves, peninsulas, and bays is most useful.

The following coastline sites were selected, and together they provide a range of useful and desirable conditions:

(a) Baja, California. This site is a desert-like peninsula surrounded by water.
(b) The northwest coast of Australia. This site has an irregular coastline with desert immediately adjacent to ocean.
(c) The coast of Libya. The Gulf of Sidra intrudes into desert regions at this site.
(d) The southeast coast of the Arabian peninsula. This site is an irregular coastline roughly parallel to the ERBS orbit ground track.

Figure 5 shows a typical plot of longwave radiance measurements as the scan track crosses a coastline. Each point represents one scanner measurement. Measurements with the higher radiance values are assumed to be land in daytime or water at night, and those with the lower radiance values are assumed to be the reverse. Thus, if there is a homogeneous land region bounded by water, a scan across the coastline boundary yields a measurement pattern similar to that shown in figure 5.

A cubic equation in latitude and longitude is fitted to each set of four consecutive points in a scan cycle. The inflection point for the equation is calculated for each of these sets of points. An inflection point is considered a coastal crossing (or boundary) if it falls between the two center points and if the total change in the values of the four measurements is larger than a threshold value. The threshold value is used to eliminate spurious inflection points caused by normal variations in the measurements. Once a coastal crossing point has been selected, its location is determined by interpolating between the latitude and longitude of adjacent measurement locations.

A collection of calculated coastal crossing points during a spacecraft pass is fitted to a digitized map of the corresponding coastline. Figure 6 shows two typical sets (one for ERBS, one for NOAA-9) of these calculated crossing points plotted on maps. The circles represent the calculated coastline crossing points, and the squares represent the subsatellite ground track during the overpass. Shown also is the spacecraft identification, the date of the data, the scan direction, and whether data period is during ascending or descending part of orbit. The rotation direction of the scan motion is clockwise as one looks down the spacecraft velocity vector of both the ERBS and NOAA-9 spacecraft in figure 6. This is always the case for the NOAA-9 spacecraft and the case for the ERBS spacecraft when configured with its X-axis pointed backward. The opposite is the case

when ERBS is configured with its X-axis pointed forward. The data error information is discussed in the next paragraph. Data from most spacecraft passes over the selected coastlines do not produce useful information because of the presence of clouds or poor thermal contrast at the time of satellite passage. However, by examining many days of data for each site, a large number of useful passes can be accumulated.

A figure-of-merit is needed to assess how well the estimated coastline matches the actual map coastline. The figure-of-merit selected is the least-squares distance between the calculated coastal crossing points and the map coordinates of the coastline. A latitude and longitude correction is applied to each crossing point in a manner which minimizes the sum of the squares of the distances from the crossing points to the map. This correction is then defined as the location error, in latitude and longitude, for the spacecraft pass. Values for this correction are shown on figure 6. It is also useful to consider the measurement location errors in a coordinate system at the Earth surface in which one axis is along the direction of scan and the other is perpendicular to the scan direction. Figure 6a shows that the least-squares latitude and longitude errors for this pass map into errors of $-0.0478°$ (approximately 5 km) in the direction of the scan (cross-track or normal to orbit ground track) and $0.0271°$ (approximately 3 km) perpendicular to the scan direction (along the orbit ground track).

Errors from a number of coastline detection passes can be plotted to depict a statistical distribution of the errors. Figure 7 presents a scatter plot for data from the ERBS spacecraft for November 1984 in which each point is the result of analyzing the coastline crossing points for a single coastline pass. The ellipse is the 95-percent probability region, computed assuming that the data have a Gaussian distribution with mean and covariance equal to that of the data. The random errors include uncertainties in calculating actual Earth locations of the radiometric measurements; but they also include uncertainties in the technique used in calculating the coastline crossing points. The random errors in the actual Earth location of the measurements, which include spacecraft position and attitude errors and instrument angle and misalignment errors, should, therefore, be bounded by such an error ellipse. The center of the ellipse in figure 7 suggests that there is a bias in the calculations of $-0.026°$ (about 3 km) in the cross-track direction and a much smaller bias of $0.0048°$ (about 0.5 km) in the along-track direction. This bias is discussed in the next section.

RESULTS AND DISCUSSION

The method presented earlier for calculating ERBE scanner measurement locations on the Earth has been implemented in the data processing software to calculate the latitude and longitude of every scanner radiance measurement. The coastline detection technique described in the last section has been applied to large numbers of coastline crossings to evaluate how accurately the calculations of Earth locations are being made. Figure 6, introduced in the previous section, shows comparisons in coastline crossing points

between actual map values and values computed using the coastline detection technique. The estimated coastline crossing points are seen to follow the actual coastlines of the California Baja peninsula and Libya quite well.

The figure-of-merit errors computed for the pass of figure 6a of 0.027° along-track and −0.048° cross-track result in errors in distance at the Earth surface of about 3 and 5 km respectively. The largest difference in distance between an individual actual and calculated crossing point for the ERBS and NOAA-9 data of figure 6 was found to be about 15 km. Since the scanner field-of-view is about 30 km at nadir, the calculated Earth locations are well within this field of view.

The distribution of errors in the calculations of the coastline crossing points for the ERBS spacecraft for November 1984 (figure 7) shows a small cross-track bias. This bias of −0.03° represents a constant error of about 3 km along the scan track in a direction which is opposite to the direction of the scan beam motion. The plot of figure 7 includes data from passes over all four different coastlines, and it includes data from cases when the ERBS spacecraft was flying X-axis forward and cases when it was flying X-axis backward. With this range of conditions, it is unlikely that the bias is caused by errors in spacecraft ephemeris or attitude data or in the method of calculating the coastline detection errors. Instead, the bias may be caused by a detector misalignment, errors in instrument elevation angles, or by the method used to account for the response of the instrument as it views a changing scene. The effect of the bias has been removed in the production processing for both the ERBS and NOAA-9 spacecraft by subtracting a constant from the value of the elevation angle before calculating each pointing vector.

Figure 8 is a plot of the measurement location errors for ERBS and NOAA-9 for April 1985. The Earth location calculations for the scanner radiometric measurements include use of the bias correction described above. The data show that the bias correction works a little better for the ERBS measurement calculations than those of NOAA-9 during this period, but the bias errors for both spacecraft are small. The error ellipses show that 95 percent of all coastline detection calculations are less than 10 km in error from the true coastline location.

Figure 9 is a plot of the measurement location errors for ERBS for December 1986. The random errors appear to be about the same as they were 2 years earlier. The data also show that the bias in calculating the scanner measurement locations on ERBS, which was discovered during the analysis of data for November 1984 is not much different than it was over 2 years ago. The agreement would be even better except for the single large error in the upper right quadrant of figure 9. This location error is caused by large errors in some of the individual coastline crossing points in the upper right corner of figure 10. These individual errors could be caused by the unusually irregular coastline or clouds in the area. This problem suggests that certain calculated coastline crossing

points need to be eliminated before deriving the figure- of-merit coastline location error for some of the coastline passes.

The first coastline location error calculations for NOAA-10, which was launched in September 1986 were made for data from November and December 1986, and the data are presented in figure 11. The random errors are larger than those seen for ERBS and NOAA-9, and there is an apparent location bias of about 12 km, most of which is along the scan axis of the instrument. This bias, however, is not normal to the ground track like the bias for ERBS and NOAA-9, because the scanner instrument on NOAA-10 normally scans in a plane which is 35° from the cross-track azimuth position. This off-normal scan mode is necessary to prevent the scanner detectors from viewing the Sun, which remains above the spacecraft horizon during most orbits. The bias shown in figure 11 is along the same axis (scan axis) and in the same direction as the bias for the ERBS and NOAA-9 spacecraft.

Sluggishness of the scan beam on NOAA-10 was observed in the data for early January 1987 and the problem became severe later in January and lasted well into February. There were times in January and February that the scan beam would come to a complete stop during the Earth scan portion of a scan cycle. The problem may have been worse than originally thought in December 1986, and this problem may account for the larger bias seen in figure 11. The problem needs further study, and it may be necessary to use biases with different values at different times, depending on the severity of the scan beam problem.

CONCLUDING REMARKS

The steps in calculating the Earth locations of the ERBE instrument scanner measurements have been described, and a coastline detection algorithm has been developed and applied to assessing the accuracy of the calculated locations. The results presented demonstrate that the ERBE scanner measurements are located within a region on the surface of the Earth which is much smaller than the field-of-view of the scanner detectors.

Most of the bias in the scanner measurement locations for all three spacecraft is aligned with the instrument scan axis and is probably not caused by errors in ephemeris and attitude data or in the method of calculating the location errors. The value of the bias for the measurements on the ERBS spacecraft appears to have remained nearly constant for the first 2 years of operation. The measurement location estimates for ERBS and NOAA-9 imply that the spacecraft ephemeris and on-board attitude data are accurate and are correctly merged with the radiation measurements. The larger bias in the location estimates for the NOAA-10 spacecraft for November and December 1986 may be caused by an observed scan beam problem and needs further investigation.

For the ERBS and NOAA-9 data analyzed, figure-of-merit coastline location errors for a coastline pass are less than 10 km, and individual location errors during a pass are less than 15 km. The average figure-of-merit coastline location error for ERBS and NOAA-9 for a month of data is less than 5 km in the cross-track and down-track direction. These errors include uncertainties in the coastline detection technique as well as errors in calculating the scanner measurement locations.

Users of the ERBE data can rely on the geographical locations of the measurements on the archival data products. The coastline detection technique presented should have application to other remote sensing instruments which scan in a cross-track plane and which can sense thermal differences between land and ocean. The technique might also be extended to a 2-dimensional method to allow coastline detection for instruments which provide nearly simultaneous measurements in both along-track and cross-track directions.

REFERENCES

1. Barkstrom, Bruce R., 1984: The Earth Radiation Budget Experiment (ERBE). *Bulletin of the American Meteorological Society*, Vol. 65, No. 11, pp. 1170-1185.
2. Kopia, L. P., 1986: The Earth Radiation Budget Experiment Scanner Instrument. *Rev. Geophys. and Space Physics*, Vol. 24, pp. 400-406.
3. Luther, M. R., 1986: The Earth Radiation Budget Experiment Non-Scanner Instrument. *Rev. Geophys. and Space Physics*, Vol. 24, pp. 391-399.
4. Smith, G. L., Barkstrom, B. R. and Harrison, E. F., 1987: The Earth Radiation Budget Experiment: Early Validation Results. *Adv. Space Res*, Vol 7, No. 3, pp. (3)167-(3)177.
5. Hoffman, L. H., Weaver, W. L. and Kibler, J. F., 1987: Calculation and Accuracy of ERBE Scanner Measurement Locations, NASA Technical Paper 2670.

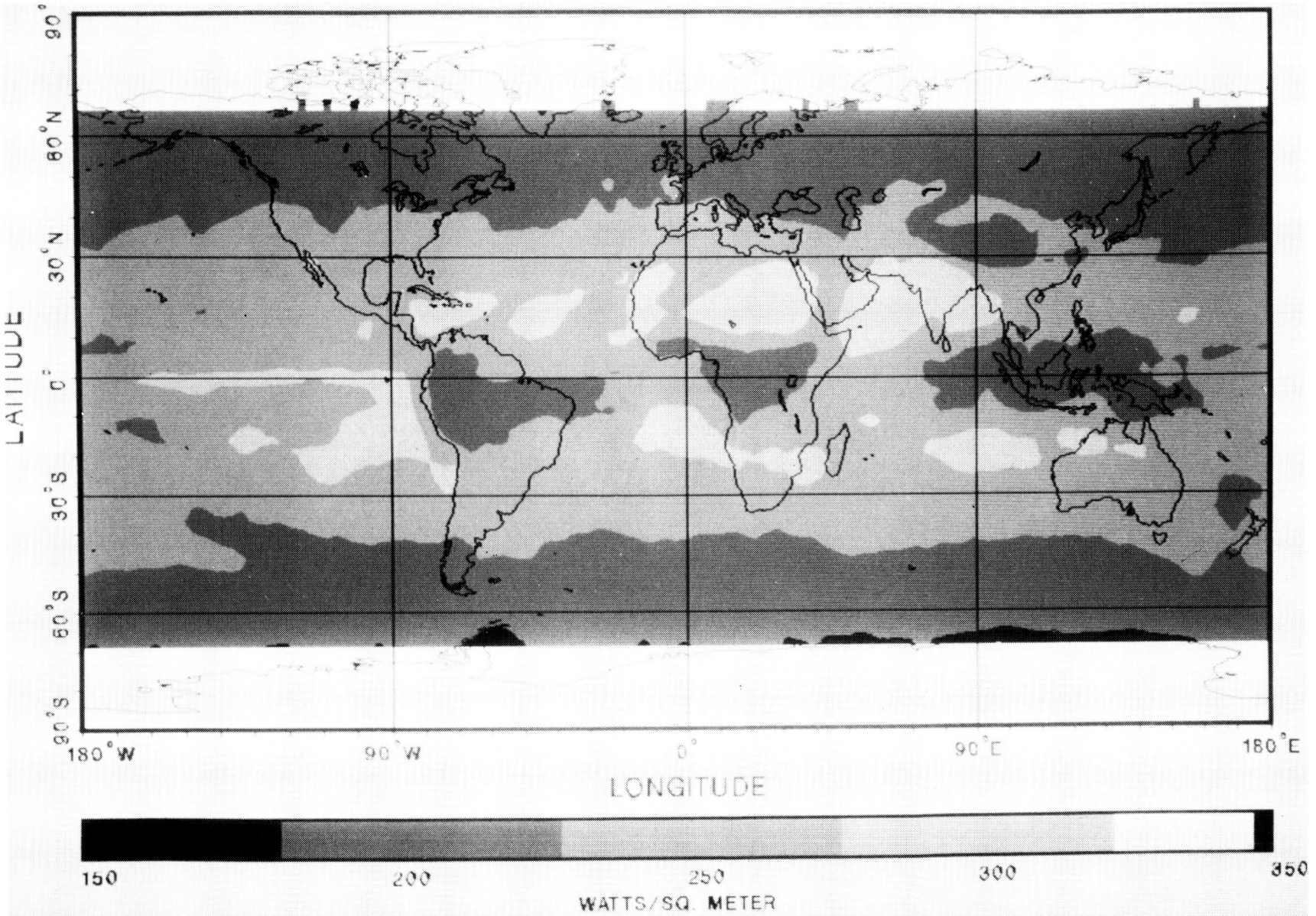

Figure 1.- Average longwave exitance for April 1985 from the ERBS spacecraft.

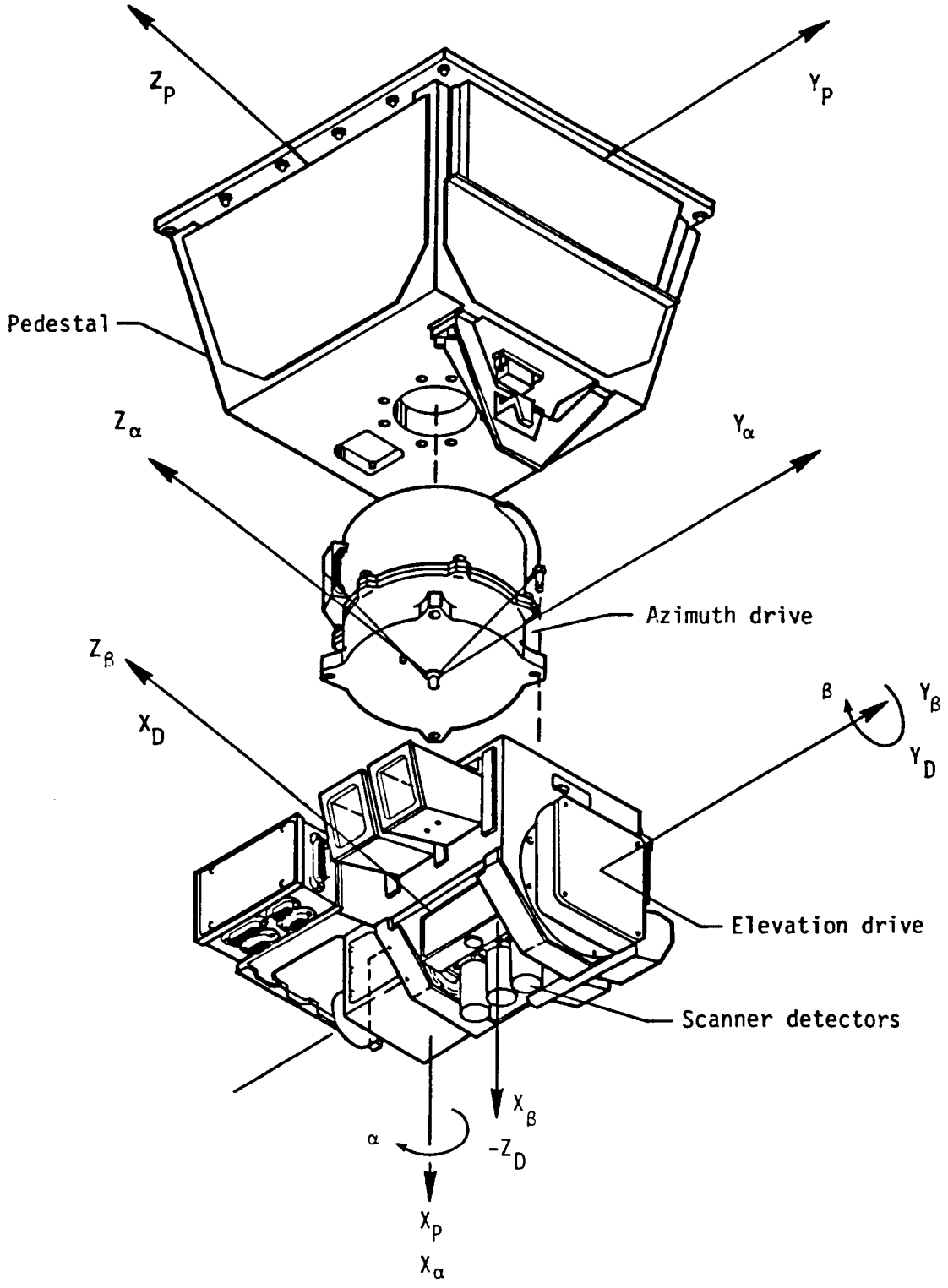

Figure 2.- Coordinate systems of ERBE scanner instrument

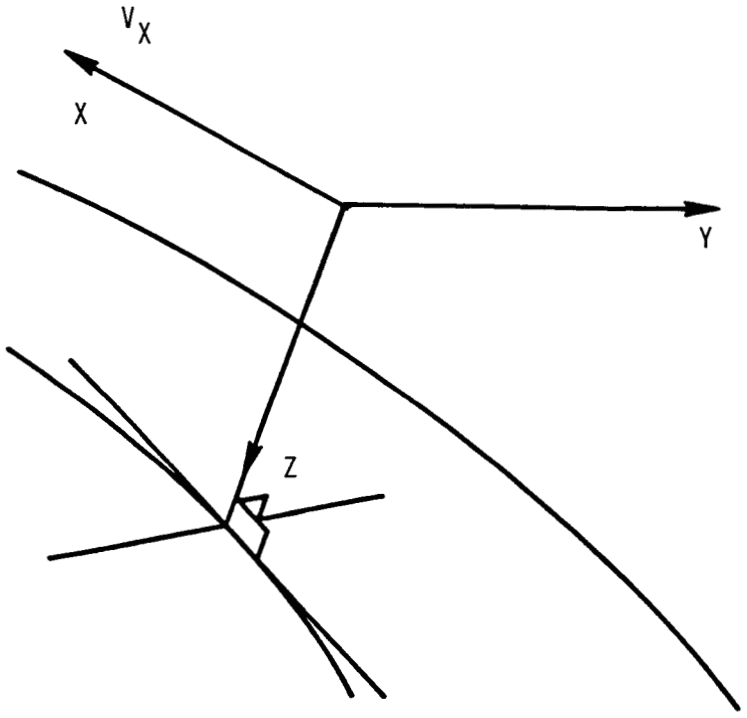

Figure 3.- Local geodetic coordinates

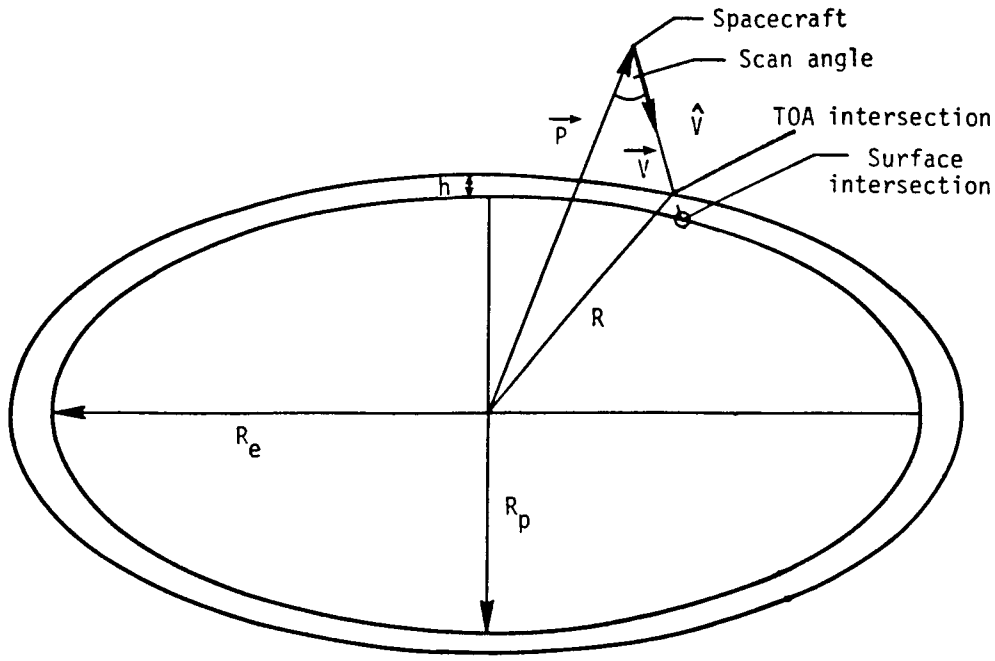

Figure 4.- Intersection of pointing vector with Earth ellipsoid.

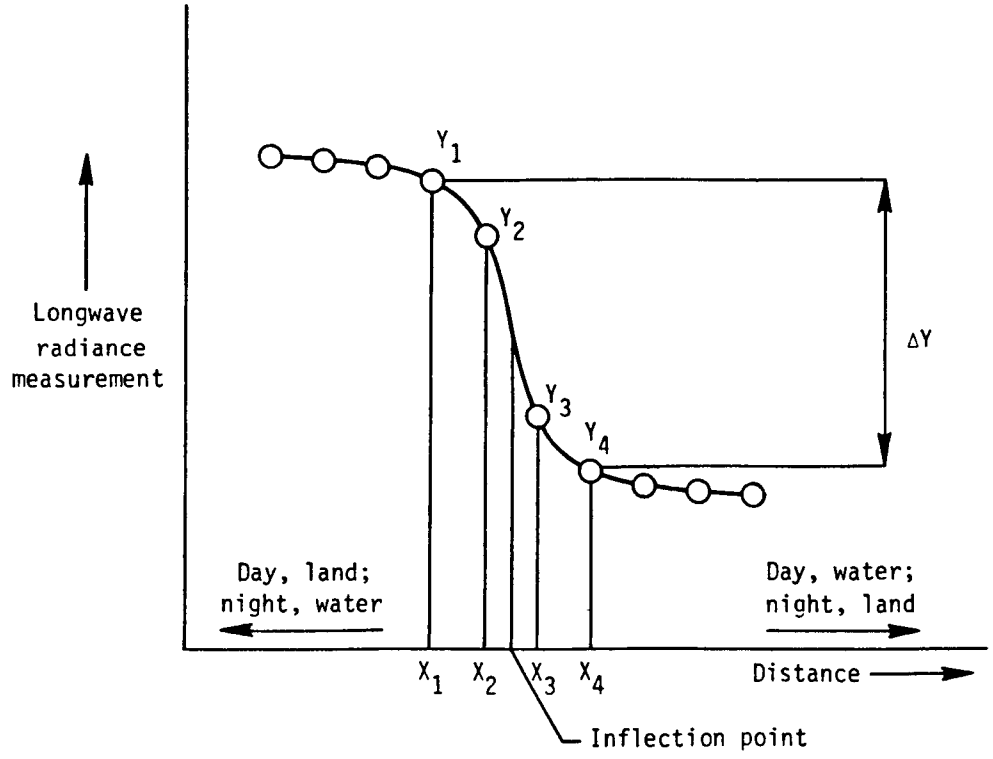

Figure 5.- Cubic fit for coastline detection.

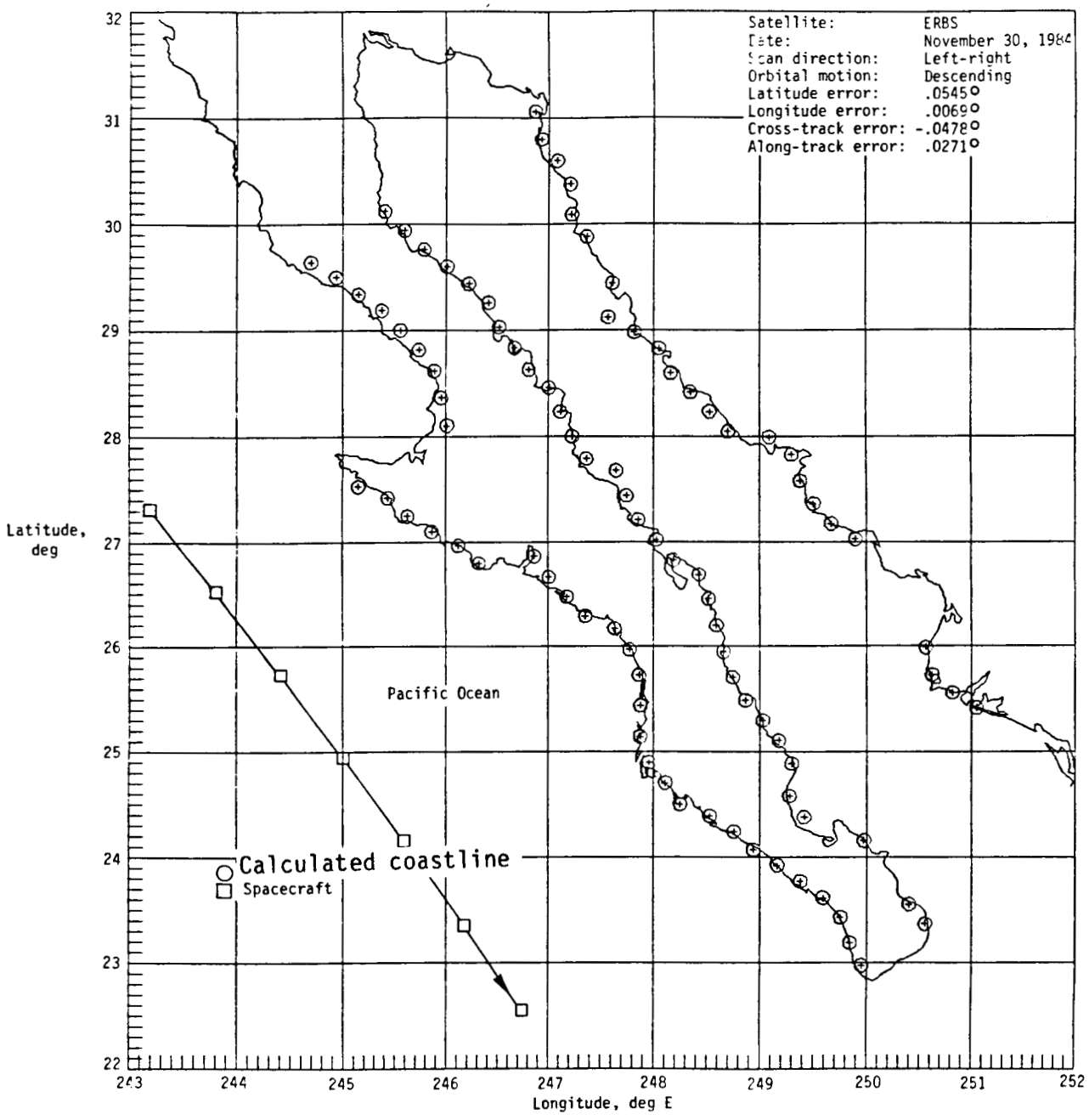

(a) ERBS over Baja California.

Figure 6.- Coastline detection results.

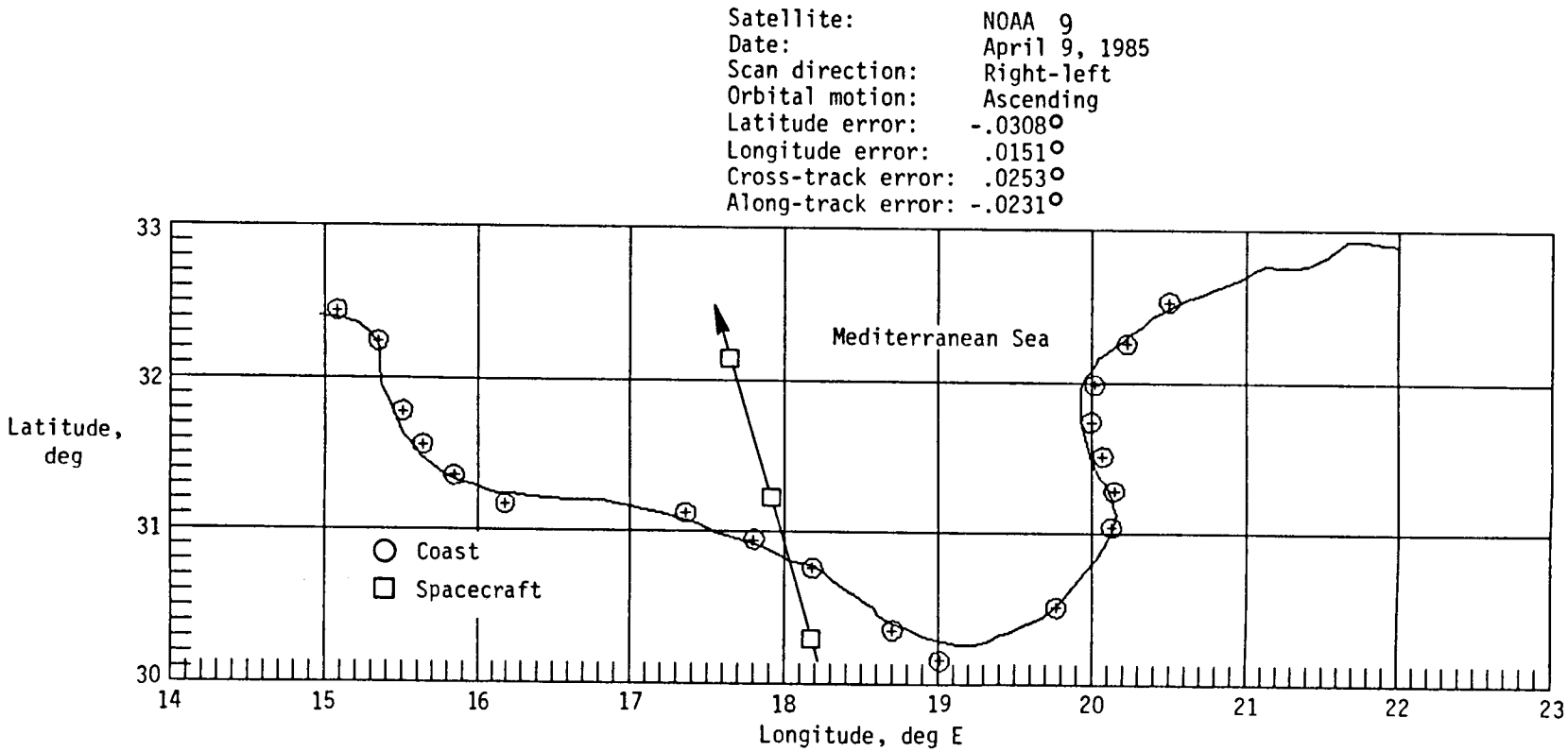

(b) NOAA-9 over Libya.

Figure 6.- Concluded.

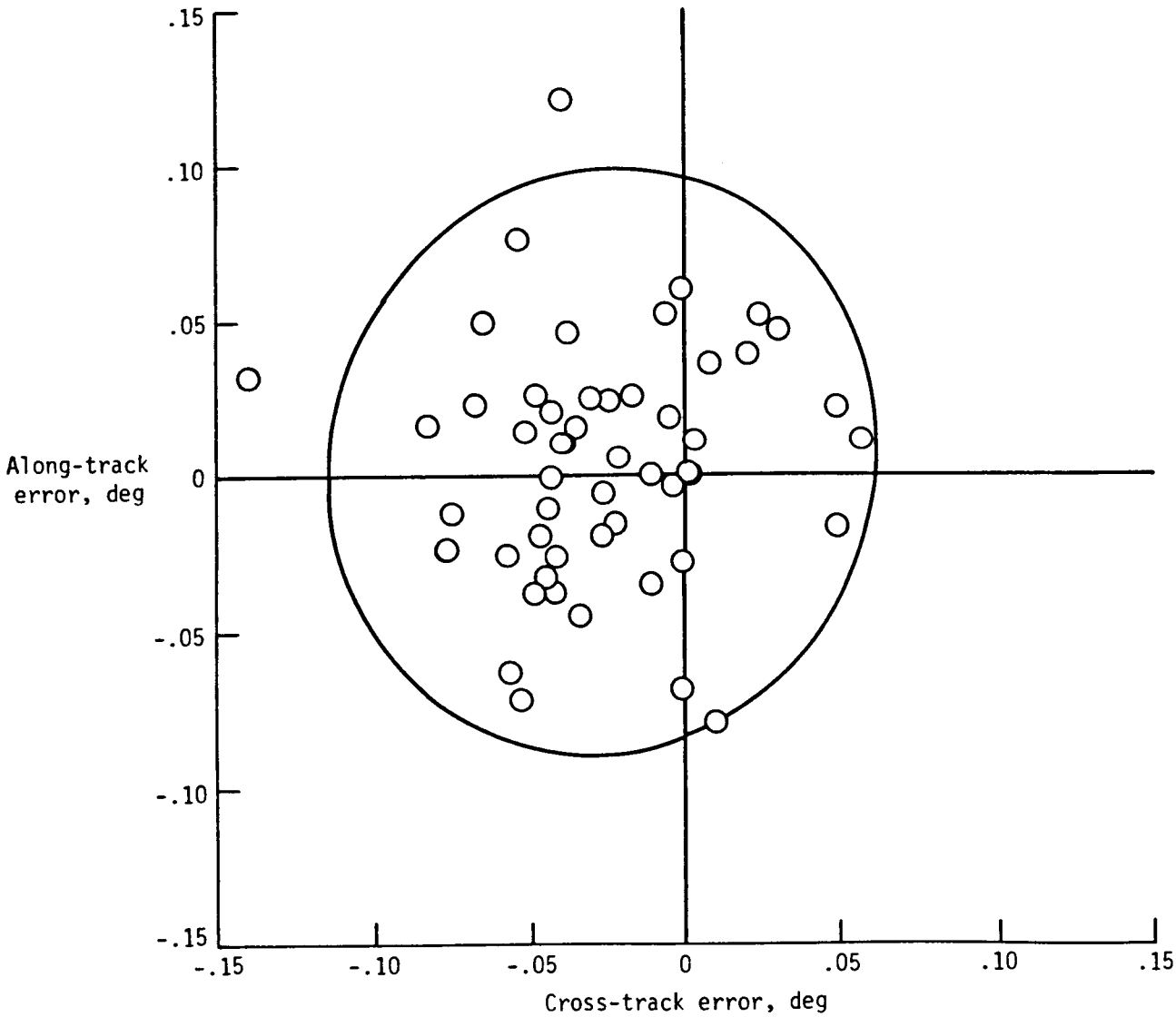

Figure 7.- Scanner measurement location errors for ERBS November 1984 showing bias.

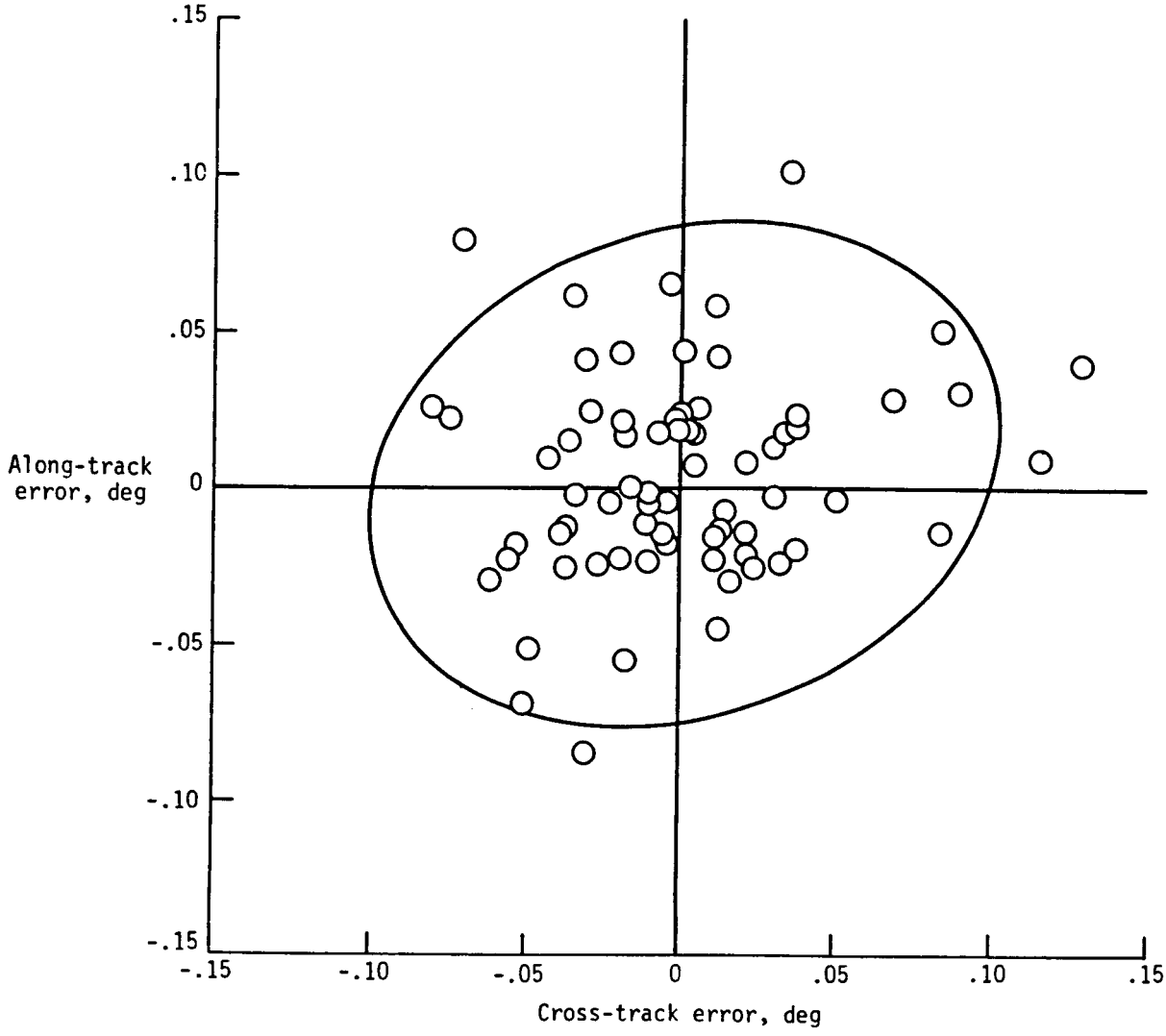

(a) ERBS.

Figure 8.- Scanner measurement location errors for April 1985.

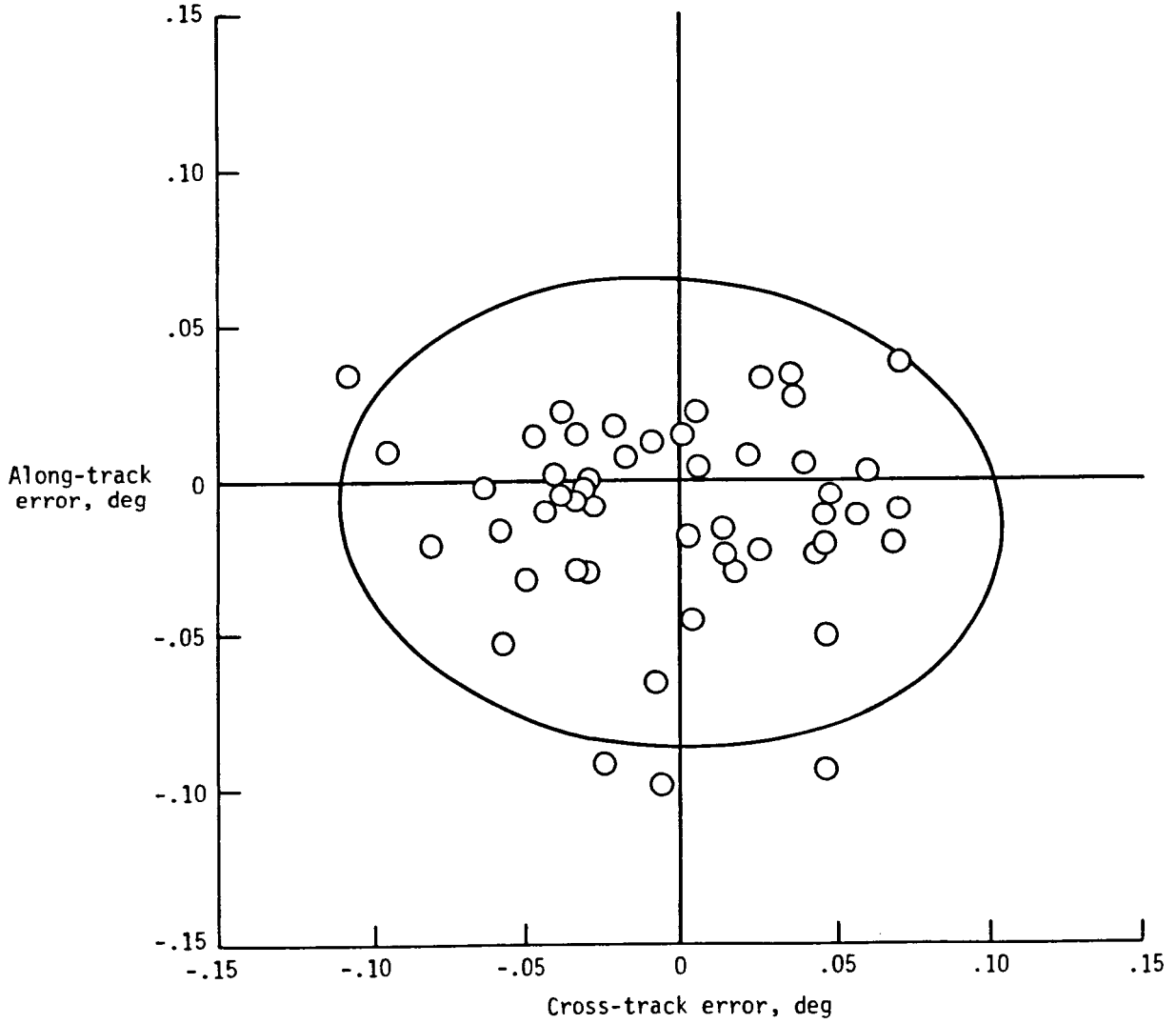

(b) NOAA 9.

Figure 8.- Concluded.

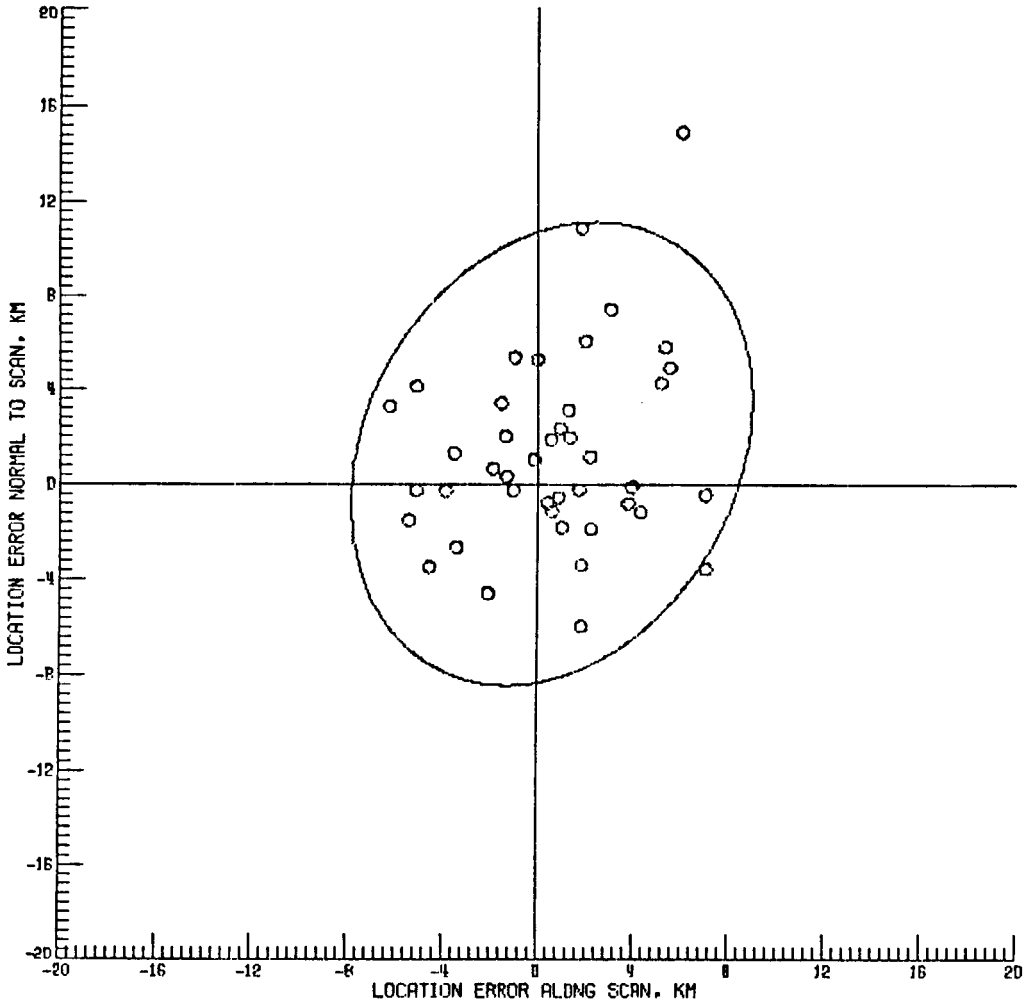

Figure 9.- Scanner measurement location errors for ERBS December 1986.

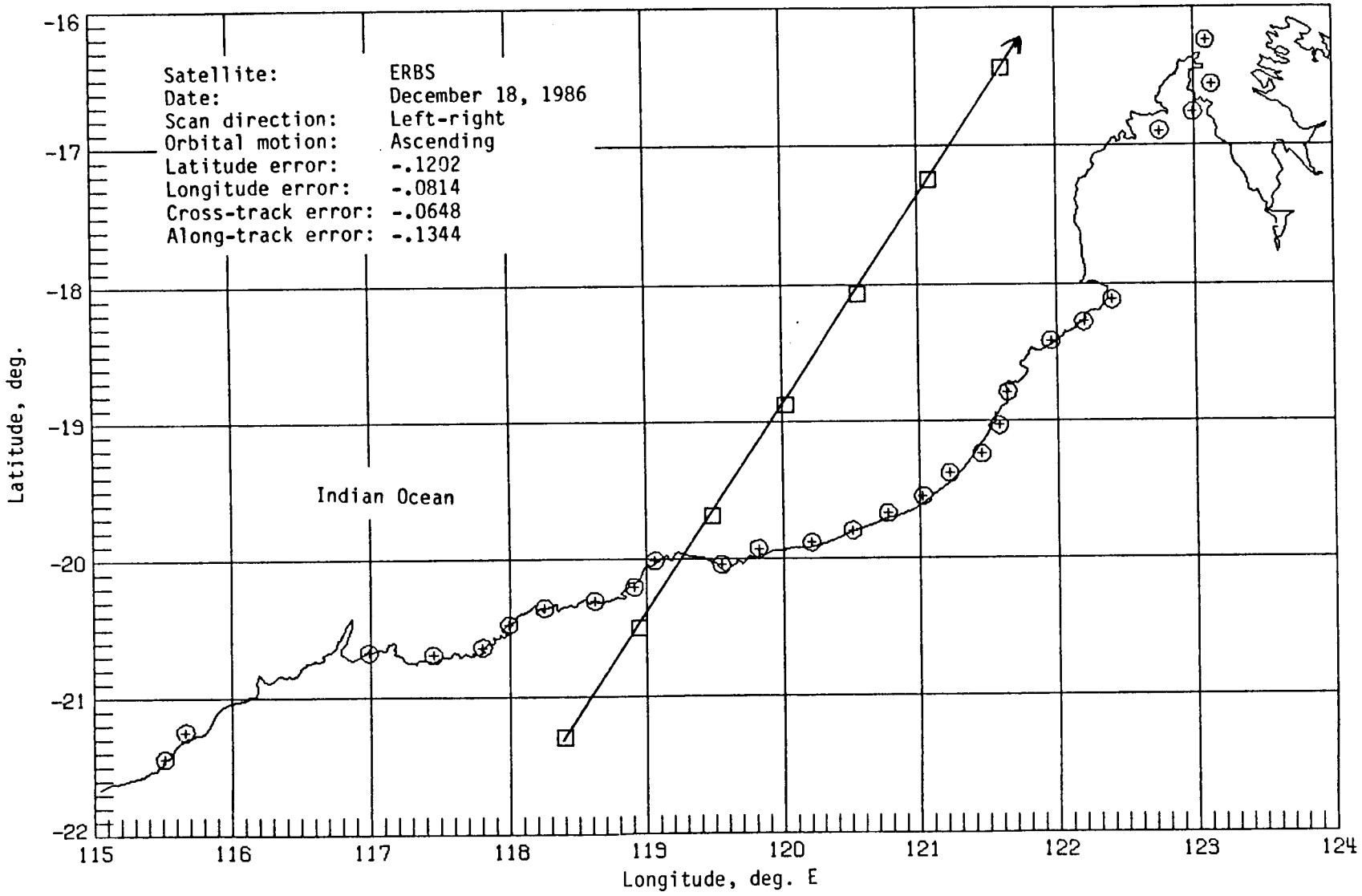

Figure 10.- Scanner measurement location errors for ERBS over Australia.

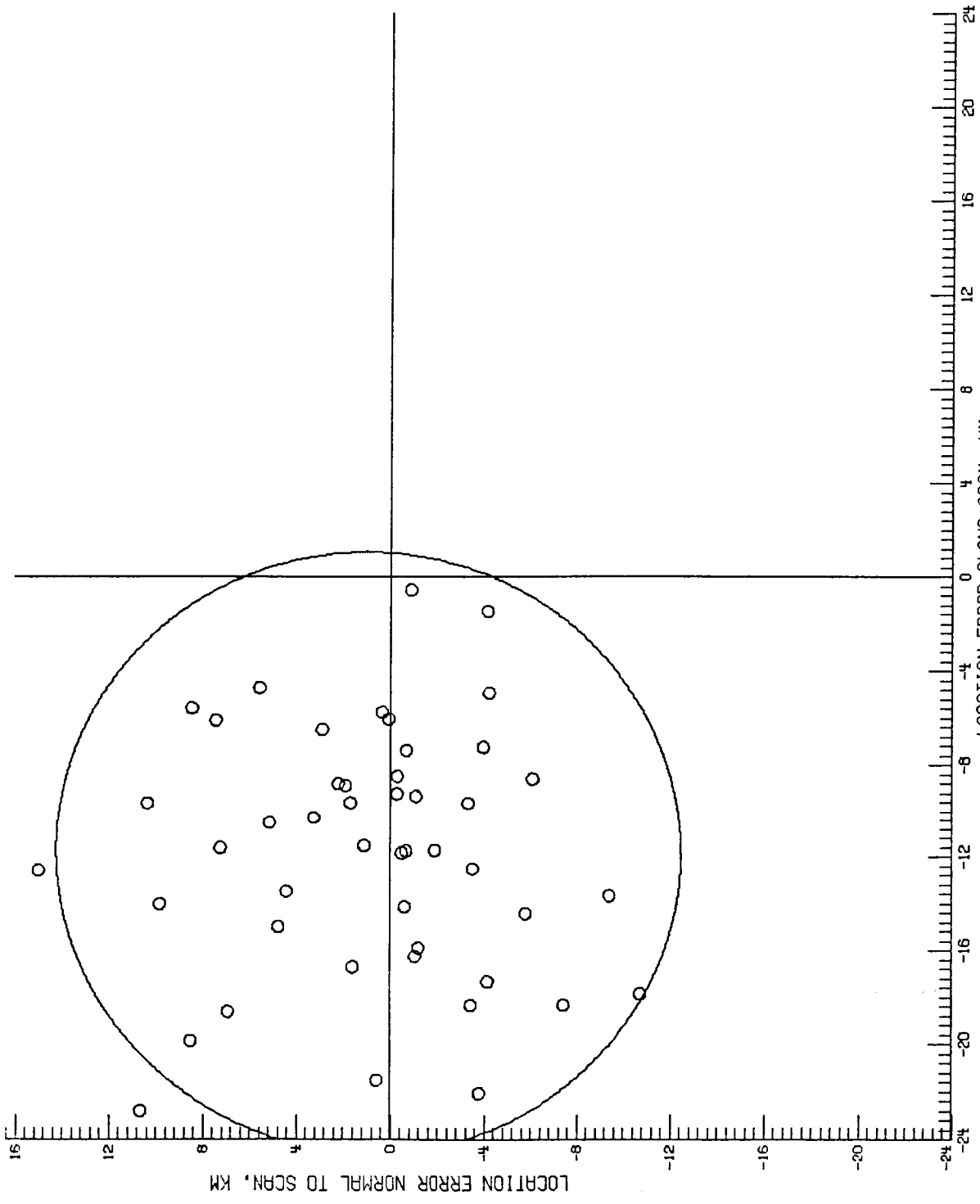

Figure 11.- Scanner measurement location errors for NOAA-10.